NUMERICAL SIMULATIONS:

WELDING INDUCED DAMAGE STAINLESS STEEL 15-5PH

基于相变场的金属材料损伤研究及工程应用

WU TONG

CHINA ARCHITECTURE & BUILDING PRESS

图书在版编目（CIP）数据

基于相变场的金属材料损伤研究及工程应用 =
NUMERICAL SIMULATIONS: WELDING INDUCED DAMAGE
STAINLESS STEEL 15-5PH : 英文 / 吴通著. -- 北京 :
中国建筑工业出版社, 2025. 4. -- ISBN 978-7-112
-30993-1

Ⅰ. TG14

中国国家版本馆 CIP 数据核字第 2025Y2X375 号

责任编辑：毕凤鸣

文字编辑：孙晨淏

责任校对：王　烨

NUMERICAL SIMULATIONS: WELDING INDUCED DAMAGE STAINLESS STEEL 15-5PH

WU TONG

*

中国建筑工业出版社出版、发行（北京海淀三里河路 9 号）

各地新华书店、建筑书店经销

国排高科（北京）人工智能科技有限公司制版

印刷厂印刷

*

开本：787 毫米 × 1092 毫米　1/16　印张：12½　字数：312 千字

2025 年 5 月第一版　　2025 年 5 月第一次印刷

定价：**76.00** 元

ISBN 978-7-112-30993-1

（44663）

版权所有　翻印必究

如有内容及印装质量问题，请与本社读者服务中心联系

电话：（010）58337283　　QQ：2885381756

（地址：北京海淀三里河路 9 号中国建筑工业出版社 604 室　邮政编码：100037）

Contents

Abstract ····· III
Contents ····· V
Nomenclature ····· IX
Chapter 1 Introduction ····· 1
Chapter 2 Martensitic Stainless Steel and Solid-state Phase Transformation ····· 6
2.1 Introduction ····· 6
2.2 Martensitic stainless steel and 15-5PH ····· 6
2.3 Phase transformation of martensitic steel ····· 9
2.3.1 Phase transformation of austenite during heating ····· 11
2.3.2 Phase transformation of martensite during cooling ····· 12
2.3.3 Main factors of influence on transformation ····· 13
2.3.4 Phase transformation models ····· 18
2.4 Austenitic grain size and its influences ····· 21
2.4.1 Grain size calculation model ····· 22
2.4.2 Effect on mechanical properties ····· 23
2.5 Measurement of phase proportions ····· 24
2.6 Phase transformation induced plasticity (TRIP) ····· 25
2.6.1 TRIP mechanisms ····· 25
2.6.2 TRIP models ····· 28
2.7 Multiphase mechanics and models ····· 31
2.7.1 Formulation of the problem ····· 31
2.7.2 Mechanical models of multiphase ····· 33
2.8 Summary ····· 38
Chapter 3 Damage Mechanics and Welding Damage ····· 39
3.1 Introduction ····· 39
3.2 Phenomenological aspects ····· 40
3.2.1 Damage variable ····· 41
3.2.2 Effective stress ····· 42

3.2.3 Strain equivalence principle ····· 43
3.2.4 Damage measurement ····· 43
3.3 Thermodynamics of isotropic damage ····· 45
3.3.1 State potential ····· 45
3.3.2 Dissipation potential ····· 48
3.3.3 Triaxiality and damage equivalent stress ····· 51
3.3.4 Threshold and critical damage ····· 52
3.4 Ductile damage models ····· 53
3.4.1 Introduction ····· 53
3.4.2 Models based on porous solid plasticity ····· 55
3.4.3 Models based on continuum damage mechanics ····· 59
3.4.4 Anisotropic damage ····· 62
3.4.5 Conclusion ····· 63
3.5 Welding damage ····· 64
3.5.1 Introduction ····· 64
3.5.2 Heat affected zone (HAZ) of weld ····· 64
3.5.3 Damage and cracking induced by welding ····· 65
3.6 Summary ····· 66
Chapter 4 Evolution Damage Multiphase Modelling ····· 67
4.1 Introduction ····· 67
4.2 Definition of damage in multiphase ····· 68
4.3 A proposed damage equation ····· 70
4.4 Constitutive equations of mesoscopic model in multiphase ····· 72
4.4.1 State potential ····· 72
4.4.2 Dissipation potential ····· 74
4.5 Constitutive equations of two-scale multiphase model ····· 76
4.5.1 Introduction ····· 76
4.5.2 Strain localization ····· 77
4.5.3 Mechanics in martensite ····· 78
4.5.4 Mechanics in austenite ····· 79
4.5.5 Memory effect during phase change ····· 81
4.5.6 Stress and damage homogenization ····· 81
4.5.7 An example in one dimension ····· 82

Chapter 1 Introduction

The research on welding, which includes thermal, metallurgical and mechanical phenomena, is a both old and new topic because many studies on the subject were started or developed many years ago and some are still going on.

The welding processes generally leaves residual stresses in the weld and its vicinity vicinity, since the solidification and contraction of molten material during cooling are constrained by the surrounding metal. The existence of such residual stresses can significantly affect subsequent lifetime by augmenting or impeding fatigue or failure events. The performance in service of parts that have been subjected to welding or heat treatment depends on the residual stress state of the structure. Consequently, for an accurate assessment of engineering lifetimes, there is a need to determine residual stress profiles. From an experimental point of view, a variety of techniques such as neutron, X-ray and synchrotron X-ray diffraction, hole drilling, curvature measurements and instrumented indentation are available to measure residual stresses[143][97][177].

Although experimental techniques provide practical solutions for measuring residual stresses, numerical methods are necessary and should be emphasized in industrial engineering. This is because design and calculation are no longer separated procedures and the calculation nowadays is already involved with the design process. Nowadays, the industrial needs in diverse fields such as aeronautics, nuclear power and automobiles impose increasingly high constraints in order to reduce manufacturing costs and to increase the reliability of parts. Control of the behavior and the rupture of mechanical structures becomes paramount with the development of simulation technology. Consequently, numerical simulation leads to various benefits for industry:

- Simulation should help avoid long test periods.
- Virtual techniques lead to maximization of performances and optimization of processes.
- Computational approaches provide additional insights into the experimental data and offer design capabilities.
- Simulation could predict and then prevent cracks or further damage induced by welding

process.

For these reasons numerical simulation plays an increasingly dominant role in certain fields of industry. It is well known that the finite element method (FEM) is a very effective approach to calculating residual stresses and damages, and increasing applications emerge in various research and industrial fields with the development of computational or electronic technology. In particular, in the field of metal hot process, virtual process becomes more popular in many institutes and enterprises to predict the results and tune the parameters before implementing the actual experiments or manufacture processes.

The history of finite element simulations of the thermal and mechanical behaviour during welding can be traced back to the 1970s[191][94][75][166][9]. Computational Welding Mechanics (CWM) is concerned with the thermo-mechanical response as well as the changes in material properties due to the thermal cycles in welding. The three most important conferences in CWM are Numerical Analysis of Weldability[2], Trends in Welding Research[1] and Modelling of Casting, Welding, and Advanced Solidification[3]. Lindgren[130] introduced different modelling aspects of the application of the finite element method to predict the thermal, material and mechanical effects of welding. Besides, he introduced the complexity of welding simulation, material modelling of welding and computational strategies of welding simulation[127][128][129].

In general, the prediction of welding residual stresses can be classified as following: statistical and empirical curves or formula, analytic method, inherent strain method[192][139][203] and thermo viscoelastoplastic finite element analysis. The first two methods are based on many simplifications and hypotheses, which lead to limited applications in industry. The concepts of inherent strain and stress were developed in Japan decades ago. This method meets the requirements of predicting welding residual stresses of carbon steels. The thermo elasto-plastic finite element analysis seems to be the most promising approach, and it has been well developed by many researchers[145][162][184][46]. In our study, we used this method to implement the models.

Therefore, our study aims to develop a numerical welding model under phase transformation including damage prediction. A successful model needs to consider thermal, mechanical and metallurgical phenomena (Figure 1.1) that are involved during the welding process. This coupled problem is usually solved by using finite element (FE) models where the thermal, mechanical and metallurgical analyses are either performed simultaneously or staggered. In prior literature[98][89][7][49],

coupling was studied between thermics and mechanism, between thermics and metallurgy as well as the influence of metallurgy on mechanics.

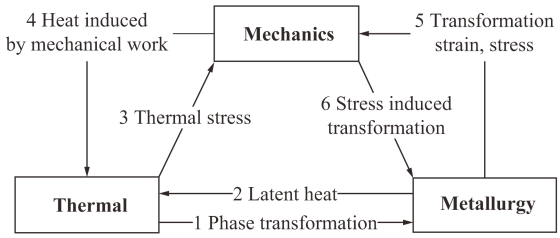


Figure 1.1 Coupling mechanisms[98]

When a model has been created, how could it be evaluated? For a successful model with application to realistic materials, one should not neglect the following two aspects: first, calibrations of parameters; second, model validations. Validation is the process during which the accuracy of the model is evaluated by comparison with experimental results whereas calibration to match the parameters with some benchmark (Figure 1.2). Thus, the same measurements should not be used for both calibration and validation purposes. An adequate model thus should have sufficient accuracy for such purpose. Here, verification is performed by assuming that the finite element model is "correct" with respect to the conceptual model and qualification is a similar process but between conceptual model and reality.

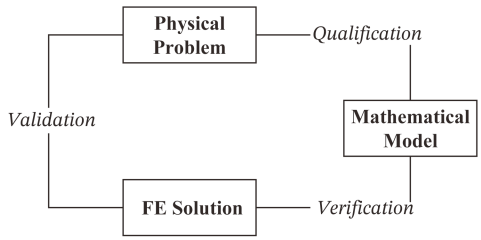


Figure 1.2 Validation and verification in finite element modeling[144]

Our work is a part of Project INZAT, which is dedicated to studying simulation and experimenting of welding of metallic materials. The project is carried out in our laboratory (LaMCoS, INSA de Lyon) and lasted more than 10 years, and is supported by various industrial enterprises of France: AREVA, EDF, EADS and ESI. Some recent work of INZAT are shown in the references[53][62][63][193][197][199][207][208][209].

Our study extends M. Coret's work that is dedicated to experimental study and numerical simulation of the welding residual stress of 16MND5 and SA533[45][46][47][48]. Another previous

Chapter 2 Martensitic Stainless Steel and Solid-state Phase Transformation

2.1 Introduction

Phase transformations often play a dominant role in the modelling of certain thermomechanical problems. General concept of thermodynamic and phase transformation is presented in[148] within the framework of solid-state physics. This chapter is dedicated not only to the mechanical behaviour and constitutive modelling but also to physical and metallurgical aspects. Introductions to concepts and models of transformation-induced volumetric strain and Transformation-Induced Plasticity (TRIP) will be found in this chapter.

2.2 Martensitic stainless steel and 15-5PH

There are three types of martensitic stainless steels: traditional (Cr13 is typical one), low-carbon and super (or soft) martensitic stainless steels. The traditional type contains 14-17wt(Cr)%[1] and 1-2 wt(C)%. Despite of its good toughness and hardness, the traditional type of martensitic stainless steels has limited application and it is thus replaced by new materials due to its low ductility and poor welding ability. The low-carbon martensitic stainless steels are melted through adding small quantity of a alloying element (e.g. Mo, Ti) and reducing the carbon content. This improves the workability and gains good corrosion resistance. Therefore, this type of martensitic stainless steel is widely applied in hydro-turbines and water pumps. The supermartensitic stainless steel with super low-carbon and low nitrogen has been developed during recent years. Its nickel content is restricted between 4% and 7%, and some alloying

1 wt( )% means weight percent.

elements (e.g. Mo, Ti, Si and Cu) are added. This type of martensitic stainless steel is well applied in pipe and oil industries. Some typical low-carbon and super martensitic stainless steels are given in Table 2.1.

Another important type of martensitic steel is a martensitic precipitation hardening stainless steel, such as 17-4PH, 15-5PH etc. Table 2.2 lists chemical integrations of some typical kinds of martensitic precipitation hardening stainless steels. The alloy investigated in this research is 15-5PH stainless steel (AMS5659), a kind of martensitic precipitation hardening stainless steels steel. It offers high strength and its common applications are components of aerospace including valves, shafts, fasteners, fittings and gears. The position of 15-5PH in metal family is shown in Figure 2.1. The specific 15-5PH which we used in experiment is H1025 (Condition H1025) which means that it is precipitation of age hardened and heat solution-treated material at specified temperature (1025°F)+/−15°F for 4 hours and air cooling. The element compositions of 15-5PH H1025 are shown in Table 2.3 (as provided by the factory). In term of microscopic scale, this steel is martensite at low temperature whereas it is in austenitic state at high temperature. The microscopic observation of 15-5PH in ambient temperature is given in Figure 2.2.

Some typical kinds of low-carbon and super martensitic stainless steels[36] Table 2.1

Type	Standard	C	Mn	Si	Cr	Ni	Mo	Others
ZG0Cr13Ni4Mo (China)	JB/T 7349-94	0.06	1.0	1.0	11.5-14.0	3.5-4.5	0.4-1.0	N,S: 0.03
ZG0Cr13Ni5Mo (China)	JB/T 7349-94	0.06	1.0	1.0	11.5-14.0	4.5-5.5	0.4-1.0	N,S: 0.03
CA-6NM (USA)	ASTM A734/ ASTM-1998	0.06	1.0	1.0	11.5-14.0	3.5-4.5	0.4-1.0	N,S: 0.03
Z4 CND 13-4-M (France)	AFNOR NF A32-059-1984	0.06	1.0	0.8	12.0-14.0	3.5-4.5	0.7	N,S: 0.03
Z4 CND 16-4-M (France)	AFNOR NF A32-059-1984	0.06	1.0	0.8	15.5-17.5	4.0-5.5	0.7-1.5	N,S: 0.03
12Cr-4.5Ni-1.5Mo (France)	CLI Company	0.015	2.0	0.4	11.0-13.0	4.0-5.0	1.0-2.0	N: 0.012 S: 0.002
12Cr-6.5Ni-2.5Mo (France)	CLI Company	0.015	2.0	0.4	11.0-13.0	6.0-7.0	2.0-3.0	N: 0.012 S: 0.002

Note: Single value means maximum.

Chemical compositions of some typical martensitic precipitation hardening stainless steels[36] Table 2.2

	C	Mn	Si	Cr	Ni	Cu	Ti	Nb + Ta
17-4PH	0.07	1.00	1.00	15.5-17.5	3.0-4.0	3.0-4.0	—	0.15-0.45

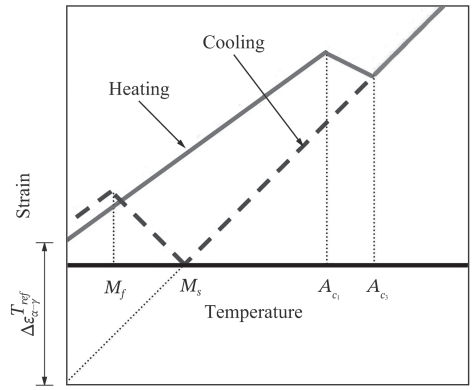


Figure 2.4 Schematic diagram of phase transformation under heating and cooling conditions

In steels, austenite can transform to ferrite, pearlite and martensite either by a reconstructive or by a displacive mechanism.

In the case of reconstructive nucleation, it is formed in the mother phase starting from local inhomogeneousness, an embryo with the composition and the crystalline structure of the new phase. The partition of the aqueous solutions to the interface between the mother phase and the embryo is supposed near to where thermodynamic balance is. In order that the transformation is carried out, it is necessary that the embryo reaches a critical size, and there is a mechanism of growth of the new phase to complete the transformation, in particular of the transport of atoms by diffusion.

In the case of displacive nucleation, it appears in the austenite of local configurations of dislocation which, by slip in a correlated way, causes the displacement of the atoms from their sites on the reticulum of the mother phase to new nearby sites which have the configuration of the crystal lattice of the new phase. The growth of the germ is carried out in the form of slats or of plates, without transport of matter at long distances compared to the interatomic distances. In steels, this type of nucleation intervenes only when, following a forced cooling, the transformation of austenite is carried out at a temperature quite lower than the A_{c_3} temperature.

Martensitic transformation is displacive and can occur at temperatures where diffusion is inconceivable within the time scale of the process. Transformation starts only after cooling to a particular temperature called martensite-start temperature or M_s. The fraction transformed increases with the under cooling below M_s. A martensite-finish temperature or M_f is usually defined as the temperature where 95% of the austenite has decomposed. Unlike M_s, M_f has no fundamental significance.

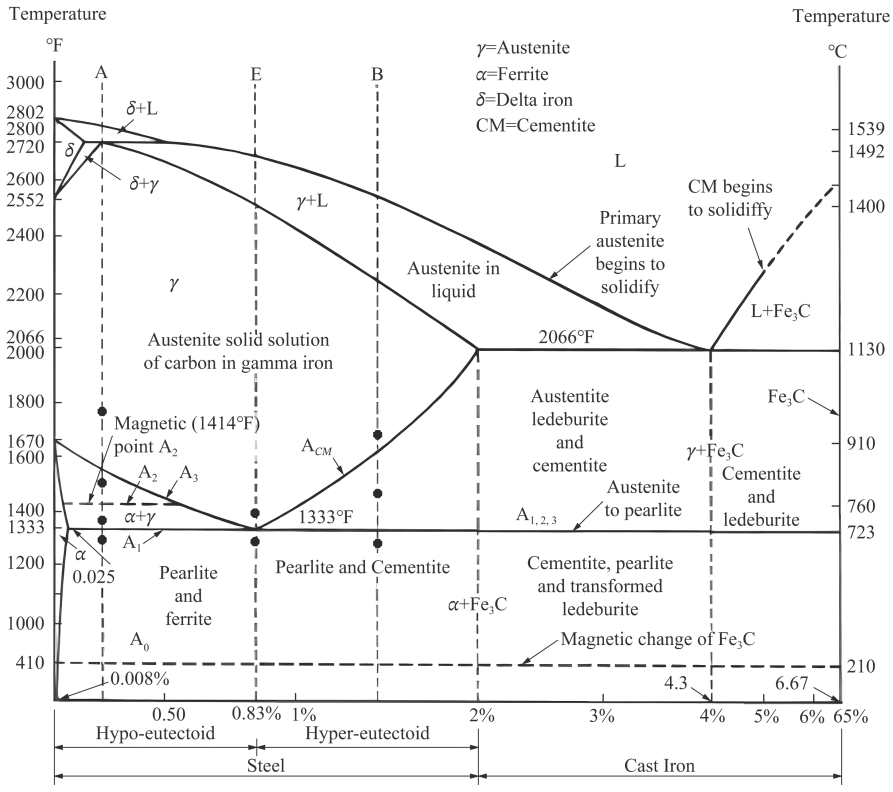


Figure 2.5 Fe-Fe_3 C phase diagram[136]

2.3.1 Phase transformation of austenite during heating

When the austenitization is processed at a sufficiently slow rate of heating under conditions of near stably thermodynamic balance, and the initial and end temperatures of transformation are respectively noted A_{c_1} and A_{c_3} (Figure 2.4). When the heating rate is faster, and the initial and end temperatures of transformation are moved towards higher values noted A_{c_1}' and A_{c_3}' and the beach of transformation is extended. Thus, the heating rate of temperature influences the kinetics of transformation and the points of beginning and end of transformation.

During the austenitization, two other parameters play an essential role: the maximum temperature reached and duration period at this temperature. These two parameters determine the parameter of austenitization which leads to a balance between time and the temperature. The higher value of this parameter means the larger size of the austenitic grain. The austenitic size of grain has an influence on the transformations during cooling. All the transformations carry out nucleation and growth. Nucleation is done preferably on discontinuities of the reticulum and for this reason,

$$\rho\Psi_e\left(T,\underline{\varepsilon}^e,D\right)=\frac{1}{2}(1-D)\underline{\varepsilon}^e{:}A(T){:}\,\underline{\varepsilon}^e+B(T){:}\,\underline{\varepsilon}^e+C(T)(T-T_0)^2 \tag{3-24}$$

where

$A(T)$: elastic tensor depended on Young's Module $E(T)$ and Poisson coefficient $\upsilon(T)$

$B(T)$: tensor related to the thermal expansion considered as isotropic

$\alpha(T)$: thermal dilatation coefficient

$C(T)$: scalar dependent on the purely thermal behavior

T_0 : reference temperature

The blocked energy by isotropic hardening can be expressed by:

$$\rho\Psi_{pi}=c(T)(1-D)\left[p+\frac{1}{\gamma}\exp(-\gamma p)\right] \tag{3-25}$$

The blocked energy by kinematic hardening is:

$$\rho\Psi_{pk}=\frac{1}{3}g(T)(1-D)\underline{\alpha}{:}\,\underline{\alpha} \tag{3-26}$$

where γ is hardening constant. $c(T)$ and $g(T)$ are hardening functions depend on material and temperature.

Therefore, the equations link between state variables and associated variables are:

$$\underline{\sigma}=\rho\frac{\partial\Psi}{\partial\varepsilon^e}=(1-D)A(T){:}\,\underline{\varepsilon}^e+B(T) \tag{3-27}$$

$$R=\rho\frac{\partial\Psi}{\partial p}=c(T)(1-D)[1-\exp(-\gamma p)] \tag{3-28}$$

$$\underline{X}=\rho\frac{\partial\Psi}{\partial\underline{\alpha}}=\frac{2}{3}g(T)(1-D)\underline{\alpha} \tag{3-29}$$

$$Y=-\rho\frac{\partial\Psi}{\partial D}=Y_e+Y_p \tag{3-30}$$

$$Y_e=\frac{1}{2}A(T)\underline{\varepsilon}^e \tag{3-31}$$

$$Y_p=\frac{1}{3}g(T)\alpha{:}\,\alpha+c(T)p \tag{3-32}$$

3.3.2 Dissipation potential

The second principle of thermodynamics or the Clausius-Duhem inequality is written as:

$$\underline{\sigma}{:}\,\underline{\dot{\varepsilon}}-\rho\left(\dot{\Psi}+s\dot{T}\right)-\vec{q}\cdot\frac{\overrightarrow{gradT}}{T}\geqslant 0 \tag{3-33}$$

where $\vec{q}$ is the heat flux vector associated with the temperature gradient.

The rate of the Helmholtz free energy is obtained by the differentiation with respect to the state variables:

$$\dot{\Psi} = \frac{\partial \Psi}{\partial \underline{\varepsilon}^e} \underline{\dot{\varepsilon}}^e + \frac{\partial \Psi}{\partial r} \dot{r} + \frac{\partial \Psi}{\partial \underline{\alpha}} \dot{\alpha} + \frac{\partial \Psi}{\partial D} \dot{D} \tag{3-34}$$

If the dissipation of thermodynamics is uncoupled with the dissipation of mechanics, we get:

$$\Phi = \Phi_m + \Phi_{th} \geqslant 0 \tag{3-35}$$

$$\Phi_m = \underline{\sigma} : \underline{\dot{\varepsilon}}^p - A_k \dot{V}_k + Y\dot{D} \geqslant 0 \tag{3-36}$$

$$\Phi_{th} = -\overrightarrow{grad} \cdot \vec{q}/T \geqslant 0 \tag{3-37}$$

Due to the plastic flow in the absence of damage (vice versa), the two inequalities are written as:

$$\underline{\sigma} : \dot{\varepsilon}^p - A_k \dot{V}_k = \underline{\sigma} : \underline{\dot{\varepsilon}}^p - \underline{X} : \underline{\dot{\alpha}} - R\dot{r} \geqslant 0 \tag{3-38}$$

$$-Y\dot{D} \geqslant 0 \tag{3-39}$$

Here, $-Y$ is a positive quadratic function, so that the damage $\dot{D}$ rate must be a nonnegative function.

The pseudo-potential of dissipation φ is then introduced:

$$\varphi = \varphi\left(\underline{\sigma}, A_k, \overrightarrow{grad}T, Y; \underline{\varepsilon}^e, V_k, T, D\right) \tag{3-40}$$

then:

$$\dot{V}_k = -\frac{\partial \varphi}{\partial A_k} \quad \text{and} \quad \frac{\vec{q}}{T} = -\frac{\partial \varphi}{\partial \overrightarrow{grad}T} \tag{3-41}$$

The pseudo-potential of dissipation is the sum of the thermal dissipation and viscoplasitic dissipation, which is coupled with damage:

$$\varphi = \varphi_{vp-d}\left(\underline{\sigma}, \underline{X}, R, D, T\right) + \varphi_{th}\left(\overrightarrow{grad}T, T\right) \tag{3-42}$$

$$\varphi_{th}\left(\overrightarrow{grad}T, T\right) = \frac{1}{2} k(T) \frac{\overrightarrow{grad}T}{T} \cdot \frac{\overrightarrow{grad}T}{T} \tag{3-43}$$

If the material properties of diffusion are isotropic, the Fourier law directly writes:

$$\vec{q} = -k(T)\overrightarrow{grad}T \tag{3-44}$$

The damage dissipation $\varphi_d(D, Y)$ could be chosen to be an exponential function[124]:

$$\varphi_d(D, Y) = \frac{S}{(s+1)(1-D)} \left(-\frac{Y}{S}\right)^{s+1} \tag{3-45}$$

where s and S are material coefficients characterizing the ductile damage evolution: they

material almost always causes hardening. At microscopic scale, hardening is characterized by an increase in the number of dislocations within material. With increasing dislocation density, they lose their mobilities. To allow accounting for this hardening, one defines a field of elasticity and studies its evolution according to the deformation. The evolution of this field can be represented by a combination of dilation, rotation, translation and distortion. Isotropic hardening is characterized by a homothetic swelling of the yield surface. In absence of distortion and on the basis of a circular surface (isotropy), isotropic hardening is then represented by the couple of scalars (r, R). Kinematic hardening is characterized by the translation of the center of the yield surface represented by a couple of tensors of internal variables $(\underline{\alpha}, \underline{X})$. Figure 4.1 shows these two hardenings when no damage occurs. The representation of hardenings with damage is given in Figure 4.2.

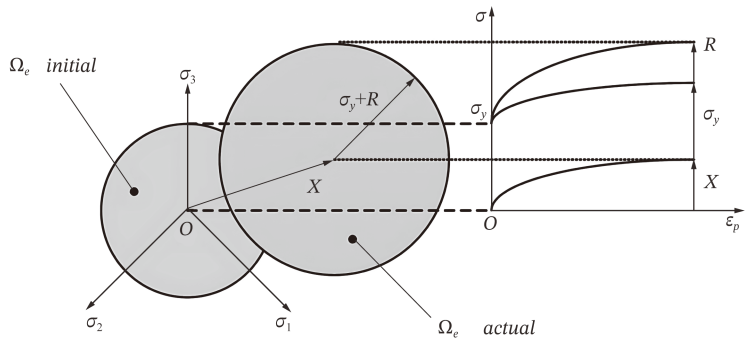


Figure 4.1 Geometrical representation of isotropic and kinematic hardenings

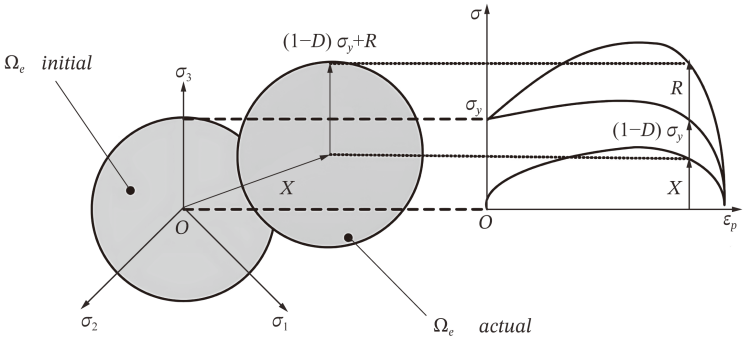


Figure 4.2 Geometrical representation of isotropic and kinematic hardenings coupling with damage

4.2 Definition of damage in multiphase

Because of assumption of isotopic and homogeneous damage, the RVE of two phases can be

presented in 2-D. We suppose that each phase has its own damage. We distinguish a mesoscale for each damaged phase from a microscale to defined damage in each scale. The damage definition in two phases is shown in Figure 4.3.

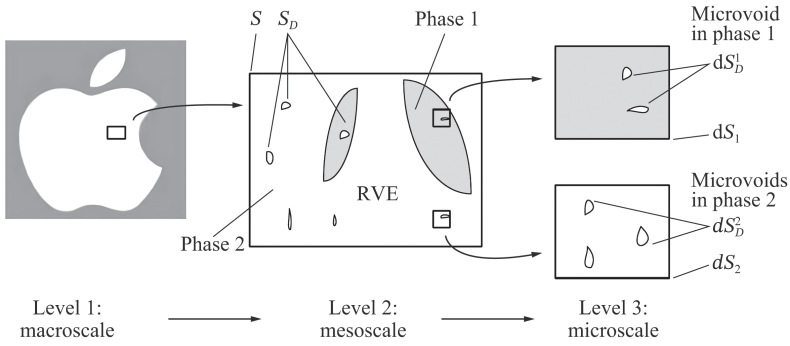


Figure 4.3 Damage definition at different scale levels

At mesoscopic scale, we neglect the fact the RVE consists of martensite (phase 1) and austenite (phase 2) and do not distinguish damage in the two phases. The damage variable is defined as the surface density of microvoides and microcracks.

$$D = \frac{S_D}{S} \tag{4-2}$$

At microscopic scale, the local damages can occur in martensite and austenite. Accordingly, the damage in phase i at microscale can be defined by:

$$D_i^u = \frac{\mathrm{d}S_D^i}{\mathrm{d}S_i} \ (i = 1,2) \tag{4-3}$$

The damage variable D in Equ. 4-2 can be divided into two parts: damage in phase 1 and damage in phase 2.

$$D = \frac{S_D}{S} = \frac{S_D^1}{S} + \frac{S_D^2}{S} = \frac{1}{S}\int_{s^1} \mathrm{d}S_D^1 + \frac{1}{S}\int_{s^2} \mathrm{d}S_D^2 \tag{4-4}$$

Introduce Equ. 4-3 into Equ. 4-4, we get:

$$D = \frac{1}{S}\int_{s'} D_1^{\mu}\,\mathrm{d}S_1 + \frac{1}{S}\int_{s^2} D_2^{\mu}\,\mathrm{d}S_2 \tag{4-5}$$

Let us define

$$D_i = \frac{1}{S_i}\int_{S_i} D_i^{\mu}\,\mathrm{d}S \ \ (i = 1,2) \tag{4-6}$$

$$\xi_i = \frac{S_i}{S} \ (i = 1,2 \quad \xi_1 + \xi_2 = 1) \tag{4-7}$$

$$D_c = \left[\left(\frac{K^2}{2ES}\right) \cdot f\left(\frac{\sigma_H}{\sigma_{eq}}\right)\right]^s \langle p_R - p_D \rangle^\kappa \tag{4-22}$$

In proportional loading cases, σ_H/σ_{eq} is a constant. Consequently, from the above two equations, we get:

$$D = D_c \left\langle \frac{p - p_D}{p_R - p_D} \right\rangle^\kappa \tag{4-23}$$

with

$$p_R - p_D = D_c^{1/\kappa} \left[\left(\frac{K^2}{2ES}\right) \cdot f\left(\frac{\sigma_H}{\sigma_{eq}}\right)\right]^{-s/\kappa} \tag{4-24}$$

If we take the initial damage D_0 of material into account, the proposed equations are written as:

In uniaxial loading:

$$D = \frac{D_c - D_0}{(p_R - p_D)^\kappa} \langle p - p_D \rangle^\kappa \tag{4-25}$$

In multiaxial loading:

$$D = \frac{D_c - D_0}{(p_R - p_D)^\kappa} \left\langle p\left[\frac{2}{3}(1+\upsilon) + 3(1-2\upsilon)\left(\frac{\sigma_H}{\sigma_{eq}}\right)^2\right] - p_D \right\rangle^\kappa \tag{4-26}$$

The damage exponent κ is a parameter of material depending on the temperature.

In fact, if we neglect the initial damage of material and κ is equal to 1 , the proposed model is simplified into Lemaitre's damage model. Compared with Lemaitre model, the constitutive equation of the proposed damage model contains two additional parameters: D_0 and κ. It includes 5 material parameters

$$P = (p_D, \quad p_R, \quad \kappa, \quad D_0, \quad D_c) \tag{4-27}$$

Identification of this model consists of the quantitative evaluation of the five coefficient characteristics by mean of tensile tests.

4.4 Constitutive equations of mesoscopic model in multiphase

4.4.1 State potential

In this section, we introduce a mesoscopic model to describe damage under phase

transformation. This damage is defined in mesoscale (Figure 4.3, Equ.4-4), i.e. there is no difference between the damage in austenite and in martensite.

The state potential of each phase is introduced through the method of local state in the thermodynamics of irreversible process. The total internal energy or the Helmholtz free energy is the sum of each phase's energy based on the linear mixture of different phases. In our study, it is restricted in isothermal process, and the totally internal energy e^{tot} consists of elastic and thermometallurgic internal energy $e^{e-th-met}$, viscoplastic (including isotropic and kinematic hardening) internal energy e^{vpi-pc} and internal energy induced by phase transformation e^{tr}. The following equations show these hypotheses:

$$e^{tot}\left(\underline{\varepsilon}^e, T, p, \underline{\alpha}, D, z_i\right) = e^{e-th-met}\left(\underline{\varepsilon}^e, T, D, z_i\right) + e^{vpi-vpc}\left(\varepsilon^e, T, p, \underline{\alpha}, D, z_i\right) + e^{tr}(T, z) \tag{4-28}$$

with:

$$e^{e-th-met}\left(\underline{\varepsilon}^e, T, D, z_i\right) = \sum_{i=1,2} \rho_i \psi_i^{e-th}(\varepsilon^e, T, D, z_i) + \rho\psi^{met}(\varepsilon^e, T, z_i) \tag{4-29}$$

$$e^{vpi-vpc}\left(\underline{\varepsilon}^e, T, p, \underline{\alpha}, D, z_i\right) = \sum_{i=1,2} \rho_i \psi_i^{vpi}(p, T, D, z_i) + \sum_{i=1,2} \rho_i \psi_i^{vpk}\left(\underline{\alpha}, T, D, z_i\right) \tag{4-30}$$

$$e^{tr}(T, z) = \rho\psi^{tr}(T, z) \tag{4-31}$$

where

$\rho_i \psi_i^{e-th}$: thermoelastic energy of phase i

$\rho\psi^{met}$: metallurgic energy during transformation

$\rho_i \psi_i^{vpi}$: blocked energy induced by isotropic hardening of phase i

$\rho_i \psi_i^{vpk}$: blocked energy induced by kinematic hardening of phase i

$\rho\psi^{tr}$: phase-transformation energy

And $\rho_i \psi_i^{e-th}$ can be defined by:

$$\rho_i \psi_i^{e-th}\left(\underline{\varepsilon}^e, T, D, z_i\right) = z_i\left\{\frac{1}{2}(1-D)A_i(T)\underline{\varepsilon}^e : \underline{\varepsilon}^e - \left[\alpha_i^{Tref}(T)(T - T_{ref}) - \alpha_i^{Tref}(T_0)(T_0 - T_{ref})\right]A_i(T)I : \underline{\varepsilon}^e\right\} - z_i C_i (T - T_0)^2 \tag{4-32}$$

$$\rho\psi^{met}\left(\underline{\varepsilon}^e, T, z_i\right) = \left(z_2^0 - z_2\right)\Delta\underline{\varepsilon}_{1-2}A_2(T)I : \underline{\varepsilon}^e \tag{4-33}$$

The blocked energy by the mechanism of the isotropic hardening coupled with the temperature is selected in exponential form:

图书印前设计制作协议书

委托方(甲方)： 中国建筑工业出版社

承制方(乙方)： 国排高科（北京）人工智能科技有限公司

书号	44663	书名	基于相变场的金属材料损伤研究及工程应用					
并列书名								
副书名								
开本	小16开	成品尺寸	184*260	制作方式	黑白	正文用纸	70g胶版纸	
光盘		原稿页码	208	照片		版印次	1	1
开式	竖开	制版书		装帧	平装胶订	责任编辑	孙晨淏	

就上述图书制作事宜，甲乙双方经协商达成如下协议：

一、周期

甲方于 2025-01-24 将原稿交付乙方，乙方在制作中须执行甲方书稿发排单的技术要求，于 2025-02-14 将校样、原稿交付甲方。

二、质量要求

① 图书设计符合发排单及设计工艺要求。

② 提校样的差错率在万分之三以内，超过标准须退回重新制作。

③ 付型时须同时提供付型样、付型文件盘。

④ 付型数字文件质量须符合我社标准及要求。

三、结算方式

付印后且符合结算周期、质量要求，凭结算单和本协议书按甲方《对外合作工价标准》结算相关费用。（必须开具增值税发票）

四、双方经济责任

1. 乙方丢失原稿，排、校质量不合格或超过规定的出版周期，甲方有权根据情况扣、减相应费用，包括索赔经济损失。

2. 乙方在未经图书出版中心相关人员允许和授权下，给编辑或作者提供设计、排版、改样、拷贝文件等服务，甲方不承担因此发生的费用及造成的任何经济损失，并保留追究责任的权利。

3. 乙方在出书一个月内将检查后的最终文件提交出版社审核、存档。

本文件一式两份，甲乙双方各执一份。经双方负责人签字、盖章后生效。本协议未尽事宜，双方协商，可另补充条款作为附件。附件与本协议具有同等效力。

五、保密约定

书稿文件（文字、图片、版式）未经出版社允许和授权，乙方不得擅自复制、外泄，不得在第三方进行文件的转换和调整。



（乙方）

（签字、盖章）

2025 年 01 月 24 日　　年　　月　　日

图书版式制作要求

社 书 号	44663	书　　名	基于相变场的金属材料损伤研究及工程应用		
丛 书 名				责　　编	孙晨洳
开本规格	小16开	成品尺寸	184*260	套书书号	
正文用纸	70g胶版纸	装帧	平装胶订	制版方式	黑白
设计要求： 责编通知发国排高科					